Proceedings 10th NUMGE 2023
10th European Conference on Numerical Methods in Geotechnical Engineering
Zdravkovic L, Kontoe S, Taborda DMG, Tsiampousi A (eds)

https://doi.org/10.53243/NUMGE2023-11

DEM modelling of screw piles as foundations for floating offshore wind turbines

B. Cerfontaine[1], M. Ciantia[2], M. Brown[2], Y. Sharif[2]

[1]*Department of Civil, Maritime and Environmental Engineering, University of Southampton, UK*
[2]*School of Science and Engineering, University of Dundee, UK*

ABSTRACT: Screw piles are efficient foundations for offshore renewable energy devices. Guidance recommends that they are installed in a perfect (pitch-matched) manner, in order to limit the soil disturbance. However, this necessitates the application of a vertical compressive (or crowd) force at their head, whose magnitude for upscaled offshore foundations is impractical or costly to impose in the field. It was shown that screw pile overflighting during installation in sand, i.e. applying more rotations than recommended for a given downwards displacement, has the potential to reduce the vertical load without degrading the foundation resistance. DEM simulations were undertaken to explore this seemingly counter-intuitive outcome. The soil domain was truncated to reduce the computational effort and the soil particles were enclosed in 7 radial rings whose displacement was independently servo-controlled. Different boundary conditions (constant stiffness radial rings, fixed walls or constant pressure) were tested. Screw piles were installed by applying constant rotation and displacement rates, then measured force and torque were compared against centrifuge experiments. The DEM simulations were shown to capture well the centrifuge results when a constant stiffness was applied. In addition, the origin of the torque and penetration resistance during installation (shaft, helix…) were identified.

Keywords: Discrete Element Method; Screw Pile; Offshore geotechnics; sand

1 INTRODUCTION

The development of offshore wind farms, necessary to reach net zero objectives, has also an environmental impact. New wind farm developments require hundreds of foundations, often piles, installed over large areas. Pile driving, the dominant pile installation method, can be harmful for marine inhabitants due to noise. Therefore, more silent pile installation methods have been developed, such as screw piles (Davidson et al. 2022; Cerfontaine et al. 2023).

Screw piles are composed of one or several helices attached to a steel shaft. They are rotated into the ground by applying a torque at their head. Screw piles are particularly suitable as foundations for jacket structures, as the helix enhances the axial capacity of the pile in both tension and compression (Cerfontaine et al. 2022; Davidson et al. 2022). Their large tensile resistance also makes them suitable as anchors for floating renewable energy devices (Cerfontaine et al. 2020).

Current design guidance for onshore screw pile recommend that, during the installation, the pile must advance of one helix pitch (p_h) per pile rotation (BS8004:2015 2015). However, the vertical compressive (crowd) force necessary to respect this guidance for offshore piles is of the order of several MN, which is impractical to achieve in the field. One way to reduce this vertical force is to overflight the pile, i.e. to apply more rotations than required (Sharif et al. 2021b; Cerfontaine et al. 2023). The degree of overflighting is measured by the advancement ratio (AR),

$$AR = \frac{2\pi v_z}{\omega p_h} \quad (1)$$

where v_z and ω are the vertical and rotation rates respectively. The pile overflighting corresponds to an AR≤1.

The overflighting mechanism and its effects on the force and torque necessary for installation is still poorly understood, let aside predicted. The objective of this paper is to reveal the effect of AR on the installation requirements via DEM simulations. These simulations will enable the identification of the force/torque components acting on each part of the pile (helix, tip, shaft) and give some insight into the installation mechanism.

2 METHODOLOGY

2.1 Centrifuge modelling

Centrifuge tests were used to validate the DEM results and are described in detail by Cerfontaine et al. (2021b), whilst the procedure is given in Davidson et al. (2022). The tests were undertaken in medium-dense sand (average relative density 52%, porosity 0.38), prepared

by dry pluviation. A solid steel pile model whose geometry is identical to the one presented in section 2.2.1 was used. The pile models were installed at 50g. Prescribed vertical and rotation rates were applied to the pile during installation while a load/torque cell recorded the vertical force and torque applied at the pile head.

2.2 Discrete Element Method (DEM)

In the DEM the soil behaviour is modelled as discrete interation of rigid paricles interacting with each other by means of contact laws. For its discrete nature it is well suited for studying both elementary behaviour of granular materials and large deformation soil structure interaction problems (Ciantia et al. 2019b). When modelling large boundary value problems spherical particles and particle scaling is often employed (Coetzee 2019). In this work all simulations were perfomed using PFC3D 6.17 (Itasca Consulting Group 2019).

2.2.1 Screw pile model

The model pile is shown in Figure 1b. The helix (D_h) and shaft (D_s) diameters were respectively 21.25mm and 11 mm (1.06m and 0.55m at prototype scale). The helix plate was 1.4mm (0.07m at prototype scale). The pile behaviour was rigid, and it was installed by imposing rotation and vertical displacement rates along its axis. The tip was closed-ended and full details can be found in Cerfontaine et al. (2021b)

2.2.2 Soil bed preparation

The DEM was used to create a virtual centrifuge environment with an enhanced gravity (model scaling factor N = 50g, with g the acceleration of gravity) to mimic the conditions of centrifuge tests. A scaling factor of 10 was applied to the particle size distribution (PSD) of the HST95 sand (properties in Table 1) to create a polydisperse sample. The particle-cell replication method (PCRM), proposed by Ciantia et al. (2018), was used to create a uniform soil bed from a representative cylindrical elementary volume (REV, D = 4.25m, H = 1.5m) at a target porosity of 0.38, which corresponds to the porosity of centrifuge tests. As detailed in Ciantia et al. (2018) after replicating the REV vertically seven times, contact forces were scaled to match the experimental stress profile of the soil bed ($K_0 = 0.47$).

2.2.3 Boundary conditions

To reduce the number of particles and computational cost, the pile to boundary distance ($2D_h$) was set to be smaller than the experimental one ($11.5D_h$) whilst a constant stiffness boundary condition was imposed to reduce the potential boundary effects. Seven cylindrical rings, represented in Figure 1a, were associated with a radial stiffnesses increase with depth. The radial displacement (u_ρ) of each cylinder was servo-controlled

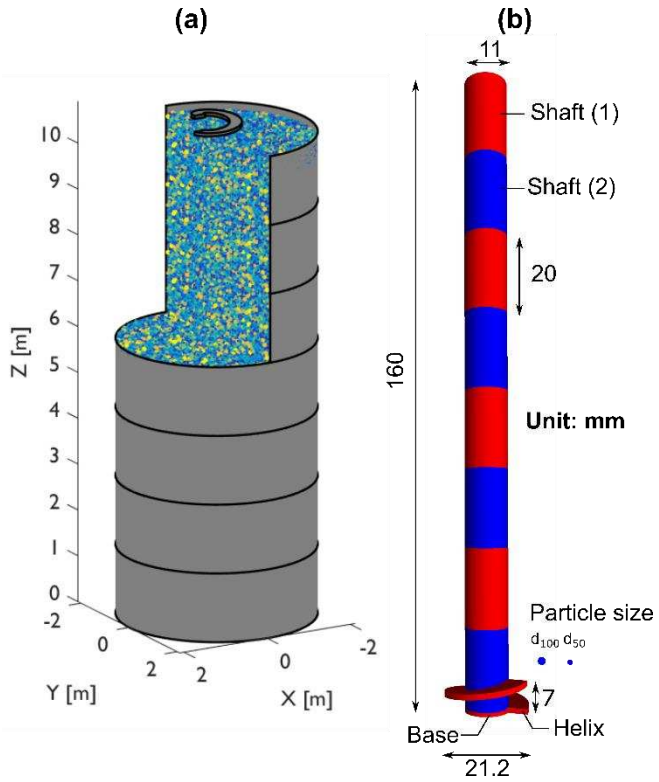

Figure 1 (a) Soil beds and servo-controlled cylinders used to impose a constant stiffness at the boundary, the helix of the pile is depicted for scale comparison. (b) Pile model and comparison with the particle size (model scale pile dimensions in mm).

with respect to its current radial position (ρ_{wall}) and was calculated based on elastic cavity expansion (Yu 2000),

$$u_\rho = \frac{\sigma_r - \sigma_{r,0}}{2G_{sand}}\rho_{wall} \quad (2)$$

where σ_r is the current average radial stress acting on the cylinder, $\sigma_{r,0}$ is the far field undisturbed radial stress and G_{sand} is the shear modulus of the sand. Both the far field radial stress and the sand stiffness are calculated at mid-depth of each cylindrical ring.

2.2.4 Contact model

Both particle-particle and pile/boundary-particle contacts were modelled using the modified Hertz-Mindlin relationship. Particle-particle contact parameters (G, ν, μ in Table 1) were separately calibrated by Sharif et al. (2019) against triaxial tests undertaken on HST95 sand used in the centrifuge tests. To properly capture experimantal stress-strain curves using spherical particles Sharif et al. (2019) inhibited particle rotation following Ciantia et al. (2019a). No further tuning of contact paramters was performed in the screw pile insallation modelling presented below. The steel-soil interface friction coefficient was assumed to be identical to the particle-pile friction coefficient (μ_{pile}). The boundary walls (cylinders in Figure 1a) truncated the soil domain, therefore the particle-wall friction coefficient for these walls (μ_{wall}) was

calculated based on the peak friction angle of the sand (~38.5°).

Table 1 Properties of the HST95 sand, after (Al-Defae et al. 2013), peak friction and dilatancy angle given at 53% relative density and DEM parameters after (Sharif et al. 2019)

Sand properties [unit]	Symbol	Value
Minimum void ratio [-]	e_{min}	0.467
Maximum void ratio [-]	e_{max}	0.769
Critical state friction angle [°]	ϕ_{cs}	32
Sand-steel friction coefficient [°]	μ_{pile}	0.445
Particle dimension [mm]	d_{10}	0.09
Particle dimension [mm]	d_{50}	0.141
Particle dimension [mm]	d_{100}	0.213
Particle density [kg/m³]	ρ_s	2650
Dry density [kg/m³]	ρ_d	1637
Buoyant density [kg/m³]	ρ'	992
Coefficient of earth pressure at rest	K_0	0.47
DEM properties [unit]		
Particle shear modulus [GPa]	G	3
Particle Poison's ratio [-]	ν	0.3
Particle friction coefficient [-]	μ	0.264

2.2.5 Installation procedure

In the centrifuge tests, the rotation rate was equal to 3 rotations per minute. However, applying this rate in the DEM simulations would lead to an onerous simulation time. Instead, it was decided to increase the penetration and rotation rates, while keeping a constant AR and quasi-static conditions. A relationship was introduced by Sharif et al. (2021) to estimate the maximum penetration rate ($v_{z,max}$) allowable to maintain quasi-static conditions:

$$v_{z,max} = \min(4p_h AR, 3D_s)\frac{I_{max}}{d_{50}}\sqrt{\frac{p'_0}{\rho_s}} \qquad (3)$$

where p_h is the helix pitch, D_s the shaft diameter, I_{max} the maximum inertial number d_{50} the average particle size, p'_0 the average initial confining stress and ρ_s the particle density. It was assumed that an inertial number equal to 0.01 was sufficient to maintain the quasi-static conditions. A discussion on the effect of penetration velocity can be found in Cerfontaine et al. (2021b). In addition, the penetration rate was increased progressively with depth, as $v_{z,max}$ is a function of p'_0 which also increases with depth. Finally, the critical time step was estimated to be 1.7E-7s.

3 RESULTS

3.1 AR effect and validation of DEM results

The centrifuge vertical force and torque measured at the pile head are depicted in Figure 2 and show the typical behaviour of overflighted screw piles, as per previous work (Cerfontaine et al. 2021; 2023; Sharif et al. 2021a). As the AR is reduced below 1.0 (overflighting), the measured vertical force in centrifuge tests changes from

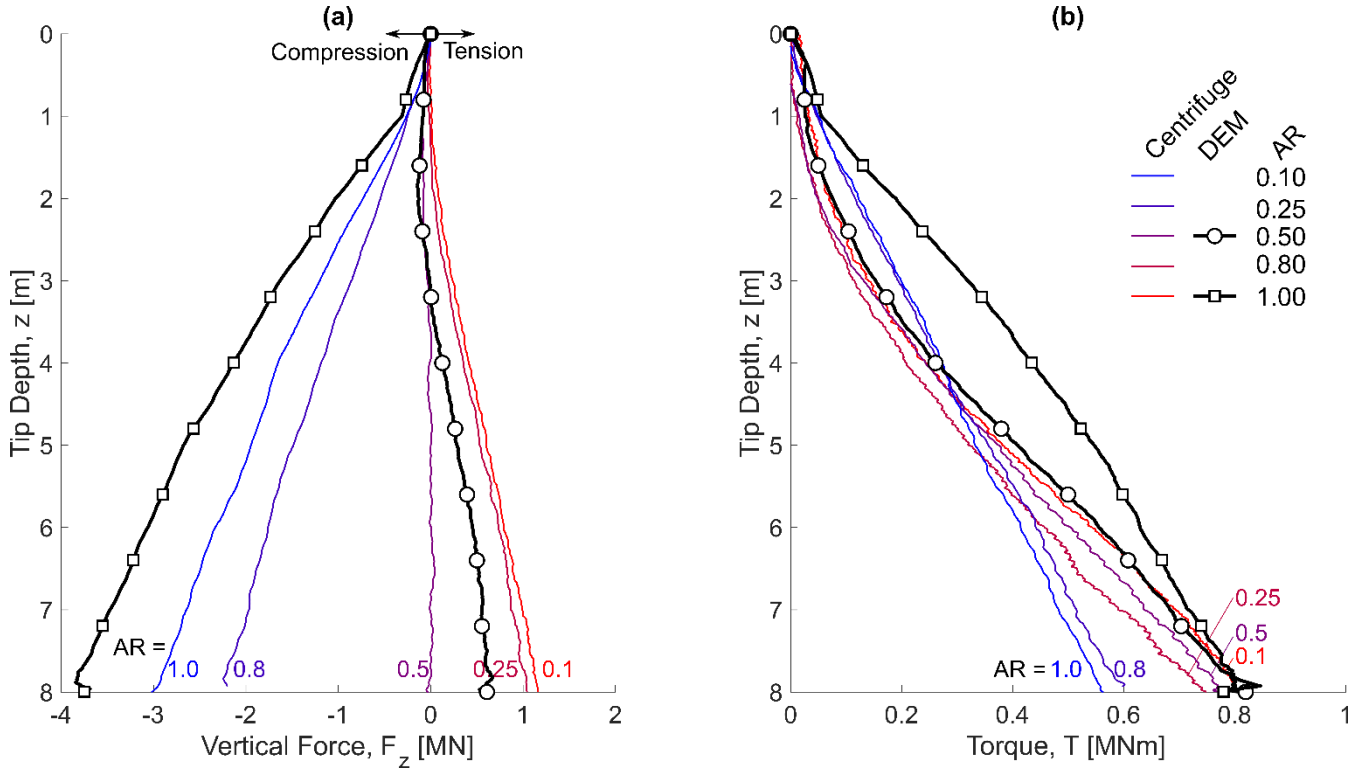

Figure 2 Comparison of results from centrifuge experiments and DEM simulations as a function of the advancement ratio (AR). (a) Total vertical force measured at the pile head. (b) Total torque measured at the pile head.

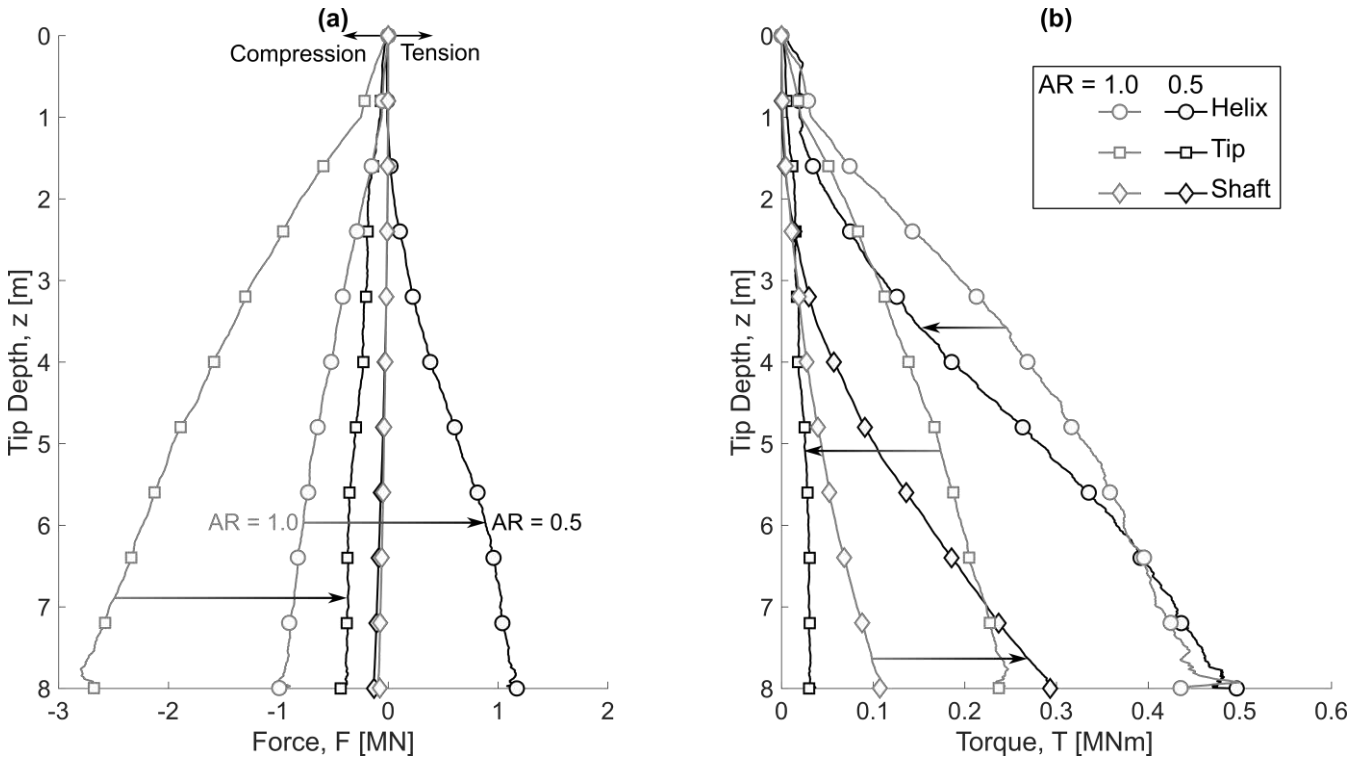

Figure 3 *Split of the measured vertical force (a) and torque (b) between the different components of the pile: helix, tip and shaft.* Results of the DEM simulations for AR = 0.5 or 1.0. Arrows indicate the change in behaviour when AR changes from 1.0 to 0.5.

compression (negative in Figure 2a) to tension at the lowermost ARs (0.25 and 0.10). The torque does not change significantly in magnitude. It ranges between 0.6kNm and 0.8kNm at final embedment depth in Figure 2b, but the depth evolution changes from approximately linear (AR = 1.0 and 0.8) to non-linear (AR≤0.5).

The DEM results show a generally good approximation of this behaviour. Only two ARs (1.0 and 0.5) were simulated and the results show the correct trend in force reduction with AR (Figure 2a), despite some overestimation of the compressive and tensile forces. The torque was slightly overestimated for AR = 1.0. However, the

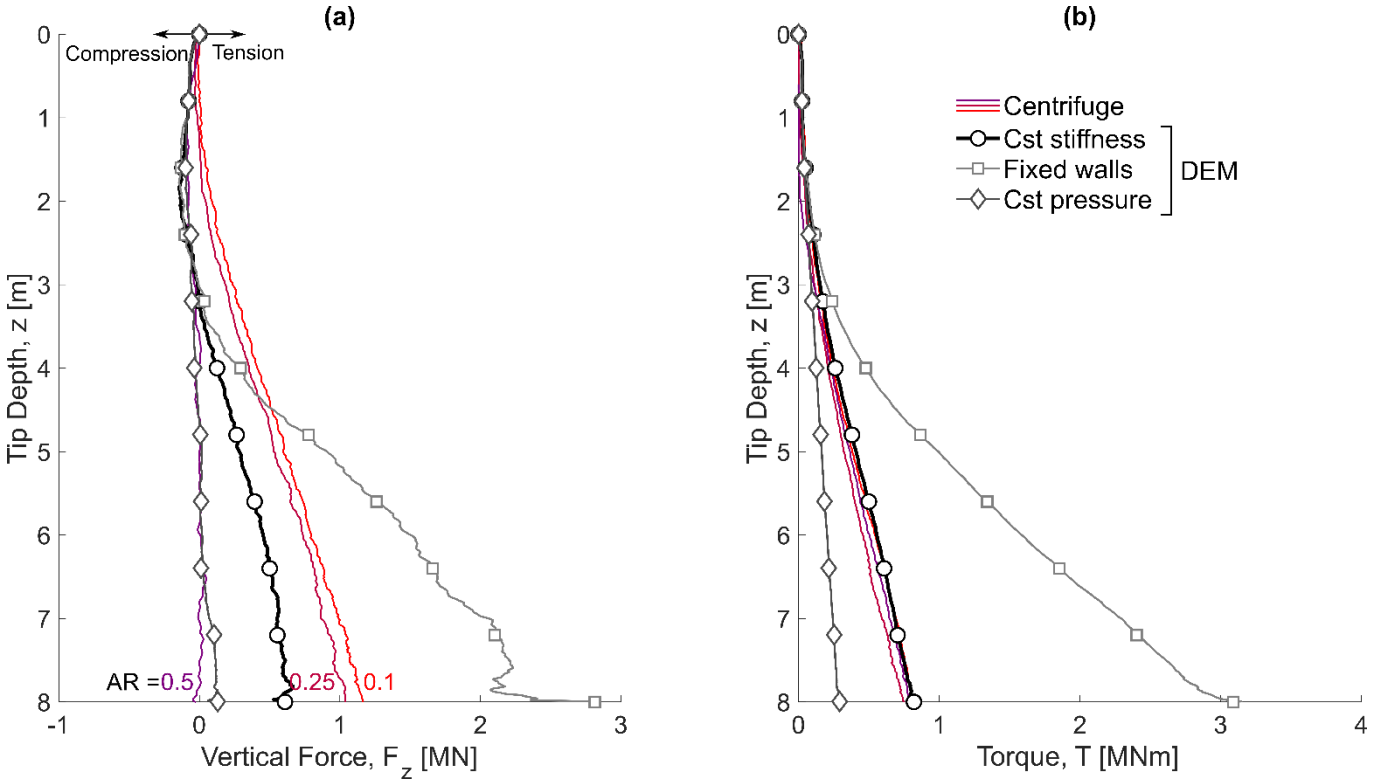

Figure 4 Comparison of boundary conditions for the DEM simulation results: (a) total vertical force; (b) total torque. Simulations for AR = 0.5. Cst stiffness = constant stiffness boundary.

linear and non-linear depth dependences associated with each AR are well-captured.

Figure 3 shows the effect of the AR on the different components of the pile (helix, tip and shaft) measured during the DEM simulations. The reduction in the total vertical force is due to two main phenomena. Firstly, the pile penetration resistance reduces significantly from approximately 3 MN to 0.4 MN. Secondly, the helix contribution changes from compression to tension. Both phenomena are consequences of the overflighting movement of the helix (Cerfontaine et al. 2021).

When AR is lower than 1.0, the helix movement forces soil particles to move upwards. The soil above the helix is then compressed similarly to a non-linear spring, which creates a force acting downwards on the upper part of the helix, i.e. the pile is pulled in and the helix is in tension (Figure 3a).

The pile penetration resistance (F_b) can be estimated generically by the following equation

$$\frac{4F_b}{\pi D_s^2} = qN_q + \frac{1}{2}\gamma D_s N_\gamma \quad (4)$$

where q is the confining stress, γ the soil unit weight and N_q and N_γ are bearing factors. By moving soil particles upwards, the helix overflighting movement reduces the confining stress under the helix. Therefore, the pile penetration resistance is reduced, with $q \to 0$ for AR changing from 1.0 to 0.5 (Figure 2a).

Figure 2b shows that even if the total torque does not change significantly, the relative contributions of the different parts of the pile actually do. At AR = 0.5, the pile tip penetration resistance reduces the maximum shear stress acting on the base of the pile during its rotation, hence the torque measured on the tip. The torque acting on the helix is approximately the same in both cases. However, the torque measured on the shaft increases as AR decreases. As the soil above the helix is compressed by the overflighting movement, the radial stress acting on the shaft in increased just above the helix. The shear stress mobilised by the pile rotation along the shaft is then enhanced, as is the torque. This is the origin of the more non-linear change in torque with depth observed in the centrifuge tests for AR<0.8.

3.2 Boundary conditions

Boundary effects can result from the truncation of the soil bed. Two additional extreme conditions were then tested to estimate the potential range of variation of the results. The first condition applies a constant stress, calculated at mid-depth to each cylinder and corresponds to a null stiffness. The second condition assumes zero radial displacement of the cylinders and corresponds to an infinite stiffness.

Figure 4 compares the results obtained with the three boundary conditions for AR = 0.5. Below 3m depth, the fixed wall leads to a more tensile vertical force and a greater torque. On the other hand, the constant pressure leads to lower force and torque. The analysis of each

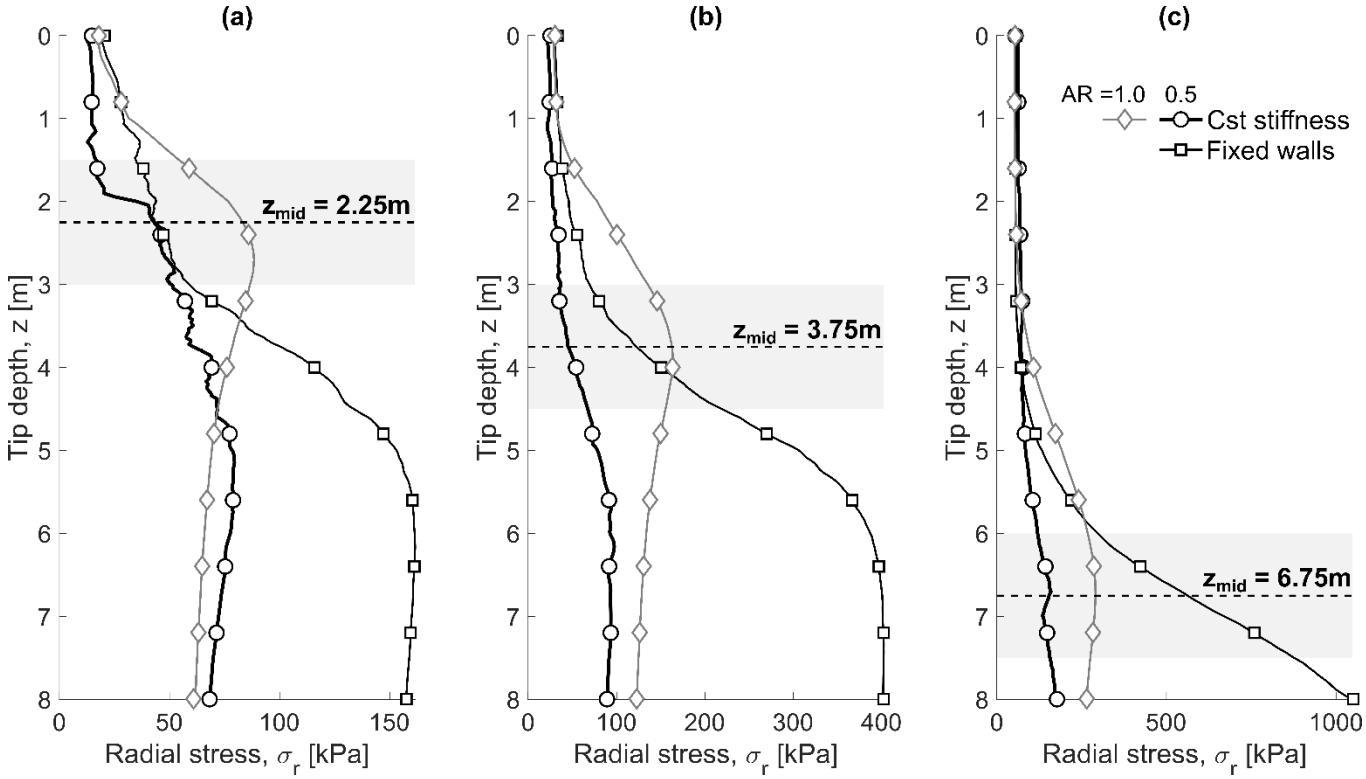

Figure 5 Average radial stress for three of the cylinders (mid-depth = 2.25m, 3.75m or 6.75m) as a function of AR and boundary conditions: AR = 0.5 or 1.0 for constant stiffness boundary (= Cst stiffness); AR = 0.5 for fixed walls. The grey zone depicts the height of the cylinder and the dashed line the average depth.

component (not shown here) reveals that the contribution of each component (helix, tip, shaft) is amplified when the radial stiffness increases, i.e. a force in compression will be more compressive. Overall, Figure 4 shows that the constant stiffness boundary conditions allows best capture of the centrifuge results.

The change in force and torque can be linked to changes in radial stress, whose average was measured for each cylinder. The change in radial stress with the pile penetration depth is depicted for three of the seven cylinders in Figure 5. The radial stress in a fixed-wall configuration is 2 to 5 times higher than in the constant stiffness configuration, hence the large torque and force.

Figure 5 also shows that the radial stress with AR = 1.0 and a constant stiffness boundary condition exhibits a marked increase in peak radial stress (up to 4 times the peak with AR = 0.5). However, the ultimate radial stress is only 50% greater from AR = 0.5 to AR = 1.0.

The change of radial stress indirectly highlights how the penetration mechanism changes with AR and described by Cerfontaine et al. (2021b). For AR = 1.0, the peak radial stress in a given cylinder is reached when the pile tip is located at it's same depth (diamond marker in Figure 5). The pile penetration forces a particle flow around the helix and induces large radial displacement of the soil. On the contrary, the peak in radial stress for AR = 0.5 is only reached when the pile is well under the position of the cylinder (circular marker). The helix movement creates a flow of particles through the helix and the uplift movement creates a failure mechanism similar to the one created for plates in tension, which typically has a conical shape. Consequently, the peak radial stress on the boundaries develops only when the pile tip reaches a deeper depth and the failure mechanism propagates upwards.

4 CONCLUSIONS

This paper investigates the effect of the advancement ratio (AR) on large screw pile installation through DEM simulations. Overall, it was shown that the DEM results capture the behaviour seen in centrifuge tests well. The paper shows how screw pile overflighting (AR <1) leads to a reduction in the necessary vertical force requirement, an increase in the shaft torque contribution and a reduction in the tip torque contribution. These changes can be explained by the helix overflighting mechanism.

The results also show that the torque and force requirements measured in the DEM simulations increase with the radial stiffness applied to the cylinder delineating the soil bed. This increase is linked to increasing radial stresses developed during the pile installation. It is therefore necessary to use an appropriate stifness to avoid boundary effects on radial stresses. The cavity-expansion based approximation here presented hence seems to be a promising approach to decreasing domain size and computational demand in DEM numerical models.

5 REFERENCES

Al-Defae, A.H., Caucis, K., and Knappett, J.A.A. 2013. Aftershocks and the whole-life seismic performance of granular slopes. Géotechnique, **63**(14): 1230–1244.

BS8004:2015. 2015. Code of practice for foundations.

Cerfontaine, B., Brown, M.J., Knappett, J.A., Davidson, C., et al. 2023. Control of screw pile installation to optimise performance for offshore energy applications. Geotechnique, **73**(3).

Cerfontaine, B., Brown, M.J., Davidson, C., Sharif, Y.U., et al. 2022. Optimised screw pile design for offshore jacket foundations in medium-dense sand. Geotechnique Letters, **12**(2): 1–13.

Cerfontaine, B., Ciantia, M., Brown, M.J., and Sharif, Y.U. 2021. DEM study of particle scale and penetration rate on the installation mechanisms of screw piles in sand. Computers and Geotechnics, **139**(11): 104380.

Cerfontaine, B., Knappett, J.A., Brown, M.J., Davidson, C., et al. 2020. Optimised design of screw anchors in tension in sand for renewable energy applications. Ocean Engineering, **217**(12): 10801.

Ciantia, M.O., Arroyo, M., O'Sullivan, C., Gens, A., et al. 2019a. Grading evolution and critical state in a discrete numerical model of Fontainebleau sand. Geotechnique, **69**(1): 1–15.

Ciantia, M.O., Boschi, K., Shire, T., and Emam, S. 2018. Numerical techniques for fast generation of large discrete-element models. Proceedings of the Institution of Civil Engineers - Engineering and Computational Mechanics, **171**(4): 147–161.

Ciantia, M.O., O'Sullivan, C., and Jardine, R.J. 2019b. Pile penetration in crushable soils : Insights from micromechanical modelling. *In* Proceedings of the XVII ECSMGE-2019. pp. 298–317.

Coetzee, C.J. 2019. Particle upscaling: Calibration and validation of the discrete element method. Powder Technology, **344**: 487–503.

Davidson, C., Brown, M.J., Cerfontaine, B., Al-Baghdadi, T., et al. 2022. Physical modelling to demonstrate the feasibility of screw piles for offshore jacket-supported wind energy structures. Geotechnique, **72**(2): 108–126.

Itasca Consulting Group. 2019. PFC3D 6.17.

Sharif, Y.U., Brown, M.J., Cerfontaine, B., Davidson, C., et al. 2021a. Effects of screw pile installation on installation requirements and in-service performance using the Discrete Element Method. Canadian Geotechnical Journal, **58**(9): 1334–1350.

Sharif, Y.U., Brown, M.J., Ciantia, M.O., Cerfontaine, B., et al. 2021b. Using DEM to assess the influence of single helix screw pile geometry on the installation requirements and in-service axial capacity in dense sand. Canadian Geotechnical Journal, **58**(7): 919–935.

Sharif, Y.U., Brown, M.J., Ciantia, M.O., Knappett, J.A., et al. 2019. Numerically modelling the installation and loading of screw piles using DEM. *In* Proceedings of the first International Symposium on Screw Piles for Energy Applications.

Yu, H.-S. 2000. Cavity Expansion Methods in Geomechanics. *In* 1st edition.